Main Manuscript for

The chloroplast ATP synthase redox domain in *Chlamydomonas reinhardtii* attenuates activity regulation as requirement for heterotrophic metabolism in darkness.

Lando Lebok[1], Felix Buchert[1]*

[1]Institute of Plant Biology and Biotechnology, University of Münster, Münster, Germany

*Felix Buchert

Email: f.buchert@uni-muenster.de

Author Contributions: L. L. and F. B. performed experiments, analyzed the data, wrote and edited the manuscript. F. B. conceived, designed, and supervised the project.

Competing Interest Statement: The authors declare no competing interests.

Classification: Biological Sciences/Plant Biology.

Keywords: ATP synthase; Redox regulation; Photosynthesis; Chlororespiration; *Chlamydomonas reinhardtii*.

Abstract

To maintain CO_2 fixation in the Calvin Benson-Bassham cycle, multi-step regulation of the chloroplast ATP synthase (CF_1F_o) is crucial to balance the ATP output of photosynthesis with protection of the apparatus. A well-studied mechanism is thiol modulation; a light/dark regulation through reversible cleavage of a disulfide in the CF_1F_o γ-subunit. The disulfide hampers ATP synthesis and hydrolysis reactions in dark-adapted CF_1F_o from land plants by increasing the required transmembrane electrochemical proton gradient ($\Delta\tilde{\mu}_{H^+}$). Here, we show in *Chlamydomonas reinhardtii* that algal CF_1F_o is differently regulated in vivo. A specific hairpin structure in the γ-subunit redox domain disconnects activity regulation from disulfide formation in the dark. Electrochromic shift measurements suggested that the hairpin kept wild type CF_1F_o active whereas the enzyme was switched off in algal mutant cells expressing a plant-like hairpin structure. The hairpin segment swap resulted in an elevated $\Delta\tilde{\mu}_{H^+}$ threshold to activate plant-like CF_1F_o, increased by ~1.4 photosystem (PS) I charge separations. The resulting dark-equilibrated $\Delta\tilde{\mu}_{H^+}$ dropped in the mutants by ~2.7 PSI charge separation equivalents. Photobioreactor experiments showed no phenotypes in autotrophic aerated mutant cultures. In contrast, chlorophyll fluorescence measurements under heterotrophic dark conditions point to a reduced plastoquinone pool in cells with the plant-like CF_1F_o as the result of bioenergetic bottlenecks. Our results suggest that the lifestyle of *Chlamydomonas reinhardtii* requires a specific CF_1F_o dark regulation that partakes in metabolic coupling between the chloroplast and acetate-fueled mitochondria.

Significance Statement

The microalga *Chlamydomonas reinhardtii* exhibits a non-classical thiol modulation of the chloroplast ATP synthase for the sake of metabolic flexibility. The redox switch, although established, was functionally disconnected in vivo thanks to a hairpin segment in the γ-subunit redox domain. Dark enzymatic activity was prevented by replacing the algal hairpin segment with the one from land plants, restoring a classical thiol modulation pattern. Thereby, ATP was saved at the expense of thylakoid membrane energization levels in the dark. However, metabolism was impaired upon silencing dark ATPase activity, indicating that a functional disconnect from the redox switch represents an adaptation to different ecological niches.

Main Text

Introduction

The chloroplast ATP synthase (CF_1F_o) is the major H^+ gate of the photosynthetic machinery (reviewed in 1, 2). Its driving force is the transmembrane electrochemical proton gradient ($\Delta\tilde{\mu}_{H^+}$) that stems from coupled photosynthetic electron transfer and H^+ movements across the thylakoid membrane. Therefore, $\Delta\tilde{\mu}_{H^+}$ consists of a membrane potential ($\Delta\Psi$) and an osmotic component (ΔpH) which both catalyze ATP synthesis (3-6). CF_1F_o consists of two parts (7, 8), a soluble (F_1 with subunits $\alpha_3\beta_3\gamma_1\delta_1\varepsilon_1$) and a transmembrane moiety (F_o with subunits $IV_1I_1II_1III_{14}$ or $a_1b_1b'c_{14}$). The electrochemical F_o motor translocates H^+ across the membrane through reversible protonations that drive the rotation of the c_{14}-ring, which is transmitted to the coupled γ- and ε-subunits. Nucleotide (de)phosphorylation takes place in the chemical F_1 motor, containing three catalytic binding pockets within the β-subunits that assume different conformations (9). This is due to steric clashes with the asymmetrical, rotating crank structure of the γ-subunit helical termini which push aside a helix-turn-helix element in the β-subunit, the DELSEED motif. Thus, the mechanical coupling of F_1 and F_o reactions facilitate the equilibration of the free energy stored in the phosphorylation potential [ATP]/([ADP][Pi]) and in the $\Delta\tilde{\mu}_{H^+}$, respectively.

With its H^+-gating function, CF_1F_o needs to be fine-tuned for optimal photosynthetic ATP output and NADPH formation efficiency at photosystem I (PSI) to sustain CO_2 fixation in the Calvin Benson-Bassham cycle. The electrochromic shift (ECS) of photosynthetic pigments has been used extensively to describe CF_1F_o activity states in vivo (10, 11, reviewed in 12). The pigment absorption changes in response to $\Delta\Psi$ and ECS decay signatures depend on ATP synthesis and ion channel activities. A poor H^+ conductivity across the membrane would generate an excessive ΔpH that counters photosystem II (PSII) efficiency and stability (13, 14), eventually affecting NADPH and ATP yields. Moreover, excessive pH-dependent nonphotochemical quenching (reviewed in 15) would become restrictive for photochemical productivity. It has also been shown that deregulated CF_1F_o favors large $\Delta\Psi$ spikes under fluctuating light that damage PSII (16). Therefore, CF_1F_o performance control in concert with other ion channels/antiporters (17, 18) are vital for optimal parsing of $\Delta\tilde{\mu}_{H^+}$ components.

Various environmental factors regulate CF_1F_o activity such as high light, drought, or CO_2 availability (19-21) but the most well-known CF_1F_o regulation involves "thiol modulation". A redox-active cysteine couple in the γ-subunit forms a disulfide that is cleaved enzymatically in the light (22-24) and restored in darkness (25). Disulfide cleavage lowers the $\Delta\tilde{\mu}_{H^+}$ threshold required for the onset of reversible ATP synthase activity (26, 27) and the dithiol formation in low light allows for efficient electron flow via a highly H^+-conductive CF_1F_o. Besides the cysteine couple, a structural determinant for H^+ conductivity tuning is a hairpin within the γ-redox domain that interacts with the β-subunit DELSEED motif (7, 28). The full scope of thiol modulation is not yet understood as mutants of the redox couple are vital in *Arabidopsis thaliana* (hereafter *A. thaliana*) (29) and *Chlamydomonas reinhardtii* (hereafter *C. reinhardtii*) (30). However, deactivating ATPase activity in the dark via disulfide formation was proposed to serve as an ATP-preserving strategy (31). Yet, in the presence of an inactive CF_1F_o, other processes are required to sustain the polarization state of the membrane, i.e., to generate a $\Delta\tilde{\mu}_{H^+}$ in darkness ($\Delta\tilde{\mu}_{H^+dark}$). The $\Delta\tilde{\mu}_{H^+dark}$ could function on several levels, such as facilitating protein import into the lumen (32) or priming CF_1F_o to surpass its $\Delta\tilde{\mu}_{H^+}$ activation threshold at the onset of light. Chlororespiration, which is important for a multitude of processes (reviewed in 33), could fulfil the requirements for sustaining $\Delta\tilde{\mu}_{H^+dark}$. Chlororespiratory electron flow occurs between NAD(P)H and oxygen by tandem action of an NADPH dehydrogenase (NDH) and a plastid terminal oxidase (PTOX), transiently storing the electrons in the plastoquinone pool. NDH activity in *A. thaliana* is electrogenic since it pumps H^+ into the lumen whereas this is not the case for the Type II NDH in *C. reinhardtii*, NDA2. Therefore, algae were speculated to sustain $\Delta\tilde{\mu}_{H^+dark}$ by ATP hydrolysis instead of chlororespiration (33, 34).

Here, ECS assays were used to demonstrate that thiol modulation in *C. reinhardtii* cells is differently functionalized than in land plants, owing to a hairpin structure that allows the alga to energize its thylakoid membranes throughout the night. We also show that algal CF_1F_o must remain active in the dark to balance the cellular redox poise via chlororespiration, which strongly depended on the trophic state of the algal cultures.

Results

1. Linking in vivo CF_1F_o activity upon dark adaptation to sequence variants in the γ-subunit redox domain.

The thiol switch from *C. reinhardtii* CF_1F_o γ-subunits displays the expected regulatory patterns in vitro and ATP synthesis rates at lower ΔpH were recorded in the reduced dithiol conformation (28). Nevertheless, we noticed under disulfide promoting conditions in dark-adapted photoautotrophic *C. reinhardtii* cultures that the enzyme was different from land plant leaves. A common in vivo method to visualize γ-subunit thiol modulation upon dark adaptation is the use of flash-induced ECS decay kinetics (29, 35). The assumption is to link a fast ECS decay to a highly active enzyme

catalyzing ATP synthesis in the presence of a γ-dithiol. Flash-induced ECS measurements were carried out in a collection of land plants and *C. reinhardtii* (Fig. 1A). All samples were dark-adapted for 30 min and, as shown in the inset, the typical three phases of the ECS kinetics were visible (reviewed in 12): The rapid ECS increase directly after the flash was attributed to PSI and PSII charge separation activity (a-phase). This was followed by a ~10-ms rise in ECS which is related to charge separation in the low-potential chain of the cytochrome b_6f complex (b-phase). Eventually, the ECS decay mainly results from ATP synthesis activity through CF_1F_o (c-phase). Clearly, the latter phase was most rapid in dark-adapted *C. reinhardtii* cells. In a next step we tested whether this might be linked to a hairpin loop in the γ-subunit that plays a role in redox regulation of CF_1F_o (7, 28). To this end we followed a segment swapping approach to assess this by genetic engineering of the γ-subunit loop. Fig. 1B shows a partial alignment of the redox domain and underlines the variations within the γ-subunit loop found in species from Fig. 1A. Moreover, the genetic sequence of the γ-subunit construct that we created to mimic a plant-like CF_1F_o in *C. reinhardtii*, termed γloop, is also listed. Fig. 1C provides the spatial reference of the aligned segment and highlights the critical position of the loop within the $\alpha_3\beta_3$ hexamer (7). It is known that *C. reinhardtii* cells establish a γ-disulfide in the dark (28) and by creating γC233S that lacks one of the redox-active cysteines we observed an accelerated c-phase in the flash ECS experiments (Fig. 1D). Importantly in Fig. 1D, dark-adapted γloop mutants showed a slow ECS decay that resembled land plant kinetics from Fig. 1A. When disulfide formation was prevented in γloop/γC233S the ECS decay was accelerated (Fig. 1D, see SI Appendix, Fig. S1 for biological replicates).

2. The natural sequence variant in the algal γ-subunit redox domain determines the dark-equilibrated $\Delta\tilde{\mu}_{H^+}$.

It is known that *C. reinhardtii* establishes the γ-disulfide in darkness which is cleaved upon illumination (28), and we confirmed thiol modulation for γWT and γloop (SI Appendix, Fig. S2 and SI Materials and Methods). The ECS decay in Fig. 1D was driven by single-turnover laser flashes that excite all photosystems, but ECS amplitudes were normalized to PSI. Accordingly, one flash perturbed the dark-equilibrated $\Delta\tilde{\mu}_{H^+}$ ($\Delta\tilde{\mu}_{H^+dark}$) by ~1.75 PSI charge separations to drive ATP synthesis activity via CF_1F_o (see also SI Appendix, Fig. S1). It is known that a large $\Delta\tilde{\mu}_{H^+dark}$ amplitude can override functional CF_1F_o restrictions imposed by the γ-disulfide (26, 27), which might account for the ECS decay differences in Fig. 1D. To address the issue, ECS-based estimations of $\Delta\tilde{\mu}_{H^+dark}$ were obtained in those samples using short saturating light pulses to catalyze multiple turnovers in the photosystems and cytochrome b_6f complex (Fig. 2A; for details of this paragraph see Material and Methods). Once the membranes were substantially energized by the light pulse, the ECS signals returned to the respective $\Delta\tilde{\mu}_{H^+dark}$ baseline within several seconds in the dark, owing to ATP synthesis activity. The initial rates of ECS generation at the beginning of the light pulse were identical (yellow symbols in Fig. 2A, SI Appendix, Fig. S3), which point to similar photochemical efficiencies after the dark adaptation. However, the ECS amplitude during the pulse varied in the CF_1F_o mutants. The variation stemmed from the fact that the respective baseline $\Delta\tilde{\mu}_{H^+dark}$ differed. This relationship – the larger the ECS amplitude during the pulse, the lower was $\Delta\tilde{\mu}_{H^+dark}$ in the sample (27, 36) – is revealed when collapsing $\Delta\tilde{\mu}_{H^+dark}$ via respiration inhibitors or uncouplers (SI Appendix, Figs. S4A-B). In the absence of inhibitors, the dark-adapted γloop in the representative measurement shown in Fig. 2A produced larger signals during the light pulse (due to lower $\Delta\tilde{\mu}_{H^+dark}$), whereas both γC233S and γloop/γC233S produced slightly smaller signals than γWT. We noticed that γC233S did hardly produce a stable ECS plateau during the pulse. The reason for this remains unknown but the ECS drifts were inducible in γWT when lowering the pulse light intensity (SI Appendix, Fig. S4C). However, the ECS plateau level at the end of the pulse was not used for the following ECS-based $\Delta\tilde{\mu}_{H^+dark}$ estimations.

Instead, the obscure $\Delta\tilde{\mu}_{H^+dark}$ baseline was estimated by referencing it to ECS_{10ms}, i.e., the measured ECS at 10 ms after the pulse that was arbitrarily defined as 0 (27, 36). Accordingly, the $\Delta\tilde{\mu}_{H^+dark}$ was expressed as negative PSI charge separation equivalents (Fig. 2B). The kinetics

comparison further revealed that the ECS decay after the light pulse was biphasic in γloop and virtually monophasic in the other strains. When treating the ECS data to quantify $\Delta\tilde{\mu}_{\mathrm{H}^+\mathrm{dark}}$ statistically, -9.9 PSI charge separation equivalents were measured in γWT, whereas the levels were insignificantly raised in γC233S and γloop/γC233S (Fig. 2C). The $\Delta\tilde{\mu}_{\mathrm{H}^+\mathrm{dark}}$ of -12.6 PSI charge separation equivalents was significantly decreased in γloop, and the difference disappeared upon uncoupler treatment where γWT and γloop showed very low $\Delta\tilde{\mu}_{\mathrm{H}^+\mathrm{dark}}$ values (SI Appendix, Fig. S4D).

The photosynthetic membranes in Fig. 2B transitioned from ECS_{10ms} (strongly disequilibrated) to $\Delta\tilde{\mu}_{\mathrm{H}^+\mathrm{dark}}$ (equilibrated) in a fashion that can be described with a two-exponential function (see SI Appendix, Fig. S5 for fitted biological replicates). Accordingly, ECS decay amplitudes were determined of the fast phase, produced shortly after the pulse, and the slow phase, produced when approaching the respective $\Delta\tilde{\mu}_{\mathrm{H}^+\mathrm{dark}}$. Both ECS decay phases represent fast and slow activity states of the CF_1F_o (37, 38). The fast phase amplitude represents the $\Delta\tilde{\mu}_{\mathrm{H}^+}$ activation threshold level that, once put in relation to ECS_{10ms}, is shown in Fig. 2D. Above the $\Delta\tilde{\mu}_{\mathrm{H}^+}$ activation level of -8.4 PSI charge separation equivalents the fast CF_1F_o was established in γWT. Very similar thresholds were determined for γC233S and γloop/γC233S. However, the active γloop CF_1F_o was established at a significantly higher level of -7 PSI charge separation equivalents.

3. The dark activity of algal CF_1F_o is entangled with metabolic flux control.

Despite the differences in darkness (Fig. 2), the less active γloop CF_1F_o was not restricting photosynthetic electron transfer nor PSI reduction during the induction phase of light-adapted cells, suggesting that a limiting ΔpH was not generated under those conditions in the light (SI Appendix, Fig. S6 and SI Materials and Methods). To get physiological insights on why the algal redox domain might have been modified, we investigated in photobioreactor experiments how *C. reinhardtii* performs under diurnal cycles and extended dark periods (Fig. 3A). The bioreactors were incubated with synchronized cell cultures and the 16-h photoperiod was carried over for two cycles. We did not detect substantial differences under photoautotrophic conditions, including the subsequent dark period (black and violet in Fig. 3A; see SI Appendix, Fig. S7 for replicates with independent transformant lines). The OD_{700nm} was set to 0.1 during the first night and the increase rate varied to some extent between transformants but did not substantially differ over the time course of the experiment. Differences were seen for the PSII quantum yields but the trend was not confirmed in the other transformants. The PSII quantum yields were inversely proportional to the light intensity and the lowest fractions of open reaction centers ranged from 0.15-0.35 at the peaking 250 µmol photons m^{-2} s^{-1}. However, during the dark phases the PSII quantum yields (here, F_v/F_m) remained stable at ~0.75 (Fig. 3A). We also examined the γWT and γloop under photoheterotrophic light/dark regimes in the presence of acetate (blue and orange in Fig. 3A, SI Appendix, Fig. S7). Here, the fraction of open PSII in the peaking light intensities was slightly increased compared to acetate-free conditions, ranging from 0.2-0.45, and the steep decline of PSII quantum yields occurred at higher light intensities. Increased PSII quantum yields in the presence of acetate are linked to diminished energy-dependent de-excitation processes. The latter could stem from diminished expression of light harvesting complex (LHC) stress-related3 protein, LHCSR3 (39), which was not further explored here. Besides LHCSR3-associated processes, the transformants in the photobioreactor showed a slight variation of their chlorophyll content (SI Appendix, Fig. S8). Smaller PSII antenna sizes as a result can therefore not be ruled out to favor higher PSII quantum yields (40) in some transformant lines. Moreover, the presence of acetate caused a mild but significant decrease in F_v/F_m under extended dark conditions in γWT – although this was not the case in all transformants (cf. black and blue in Fig. 3A and SI Appendix, Fig. S7). Importantly, a consistent effect of acetate that also differed from γWT was seen in all γloop transformants (cf. violet and orange in Fig. 3A and SI Appendix, Fig. S7): The F_v/F_m declined significantly in the mutant in an oscillating pattern which loosely aligned with the previous photoperiods. However, this effect phased out during the second day in the dark and sporadic increases of F_v/F_m were observed. F_v/F_m

recovery in γloop coincided with cell growth arrest, which we attribute to depletion of acetate in the medium. The time of growth cessation varied in the transformants, but the F_v/F_m reversion was exclusively seen in γloop. We also noticed that the onset of declining F_v/F_m and the reversion of the effect coincided with the respective rise and relaxation of F_0, the basal chlorophyll fluorescence (SI Appendix, Fig. S9). This points to a reversible reduction of the plastoquinone pool (41) and the metabolic F_v/F_m signature in heterotrophic γloop prompted us to investigate chlororespiration mutants in this experimental context. Indeed, a virtually coinciding recovery of low F_v/F_m and a stagnation of cell growth upon acetate depletion was also observed in *ptox2* mutants (Fig. 3B, SI Appendix, Fig. S10). The reduction of the plastoquinone pool in the dark in the absence of the major plastoquinol oxidase PTOX2 strongly depended on the availability of fixed carbon in the form of acetate (cf. green and olive in Fig. 3B and SI Appendix, Fig. S11). The reduced plastoquinone pool triggers state transitions upon STT7 kinase activation and migration of phosphorylated LHCII towards PSI (reviewed in 42), lowering F_v/F_m. The extent of F_v/F_m recovery upon acetate depletion, however, was less pronounced in γloop vs. *ptox2*.

Discussion

Escaping thiol modulated activity regulation due to the natural sequence variant in the algal γ-subunit redox domain.

The entanglement of thiol modulation – i.e., the reversible γ-disulfide cleavage – and the $\Delta\tilde{\mu}_{H^+}$ required to drive ATP synthesis has been consistently shown in liposome reconstitution assays from spinach (26) and *C. reinhardtii* CF_1F_o (28), as well as in *A. thaliana* leaves (27). It is consensus that the oxidized γ-disulfide conformation requires a higher $\Delta\tilde{\mu}_{H^+}$ to be active. However, published data suggests that thiol modulation by itself is less efficiently realized in *C. reinhardtii*. Hisabori and co-workers showed in in vitro experiments from *A. thaliana* that the half-time of γ-disulfide cleavage by recombinant *f*-type thioredoxins is about 1 min (43). The group has also conducted these experiments in the *C. reinhardtii* context, showing that half reduction took about 7 min (28). These studies (28, 43) also report a much slower γ-disulfide cleavage in dark-adapted algal cells vs. *A. thaliana* leaves, using the same light intensity (half reduction in vivo ~65 s vs. ~10 s in *A. thaliana*). However, unlike the high AMS labeling efficiency for the *A. thaliana* γ-subunit in the light as a full γ-disulfide cleavage indicator, the labeling efficiency was somewhat lower in the previous algal study (28), which resembled our findings (SI Appendix, Fig. S2). This raises the question why the algal system tolerates a slower, less efficient redox tuning of the chloroplast ATP synthase?
Here, we have demonstrated in vivo that the typical thiol modulation concept has been attenuated in dark-adapted *C. reinhardtii* cells via its intrinsic hairpin segment from Figs. 1B and 1C. The conclusion is based on the observation that the ECS kinetics of dark-adapted γloop algae resemble those from spinach and *A. thaliana* (27, 35, 36). In contrast, the $\Delta\tilde{\mu}_{H^+}$ activation level of algal CF_1F_o remained relatively low, whereas it was raised by 1.4 PSI charge separations in the plant-like γloop (Fig. 2D). The mutant $\Delta\tilde{\mu}_{H^+dark}$ dropped by 2.7 PSI charge separation equivalents (Fig. 2C) as a result of a larger pool of slowly active CF_1F_o. The latter produced a larger amplitude of the slowly decaying ECS in Fig. 2E which also explains the flash kinetics in Fig. 1D. Therein, both reaction centers produced less than 2 PSI charge separations after the flash as the driving force for ATP synthesis. Only the slow γloop CF_1F_o operated far below its $\Delta\tilde{\mu}_{H^+}$ activation threshold, unlike γWT and both γC233S variants. One possible explanation of the lower $\Delta\tilde{\mu}_{H^+dark}$ in γloop could be that ATPase-driven lumen acidification in the dark is not sufficient to counter passive ion leaks. Trans-thylakoid H^+ pumping that relied on the free energy in the phosphorylation potential [ATP]/([ADP][Pi]) was also depending on mitochondrial activity in the dark (SI Appendix, Fig. S4A). Yet, γloop was inactive despite the available ATP which might relate to a transient inhibition by tightly bound Mg-ADP that is favored under disulfide conditions (44, 45). The affinity of *C. reinhardtii* wild type CF_1F_o for ADP is substantially lower than in spinach (46) and it remains to be tested

whether this is due to the hairpin segment. Likewise, future efforts of increasing the available stromal ATP might yield an active γloop in the dark, e.g., through ATP import engineering (see next Section). From a mechanistic view, it is possible that the wild type algal loop segment attenuated the rotational constraints despite the γ-disulfide (Fig. 1B, underlined). The involved salt bridges between the critical arginine of the stationary βDELSEED loop and the γ-glutamate position 256 and were less stable (but not in γloop), thus attenuating the proposed chock that blocks rotation (7).

Entangling metabolic fluxes with dark activity of *C. reinhardtii* CF_1F_o.

Based on the photobioreactor analyses, the plastoquinone pool appeared to be a dead-end in γloop (SI Appendix, Fig. S9). Fig. 4 summarizes our current hypotheses of misregulated metabolic pathways in the mutant, all of which remain subject of active research. Although other processes may be relevant, such as starch metabolism or protein import, the current dataset suggests that chlororespiration is affected in γloop after silencing dark ATPase activity. Chlororespiration (reviewed in 33) may assist in membrane polarization in vascular plants where NDH is electrogenic and dark ATPase activity is low. Contrary, dark ATPase activity via CF_1F_o may be a chlororespiratory prerequisite when a non-electrogenic NDH is involved, such as *C. reinhardtii* NDA2 (47). When there is an excess of ATP in the cytosol in the dark, heterotrophic *C. reinhardtii* cells import ATP into the chloroplast at the cost of co-importing NAD(P)H (reviewed in 48). In support of previous work on algal chlororespiration (49, 50), acetate-fueled mitochondrial respiration in Fig. 3 delivered the stromal electrons that were transiently stored in the plastoquinone pool in dark aerated cultures. Accordingly, chlororespiratory oxidation of the plastoquinone pool might sustain cytosolic ATP import. Various cellular signals might be disturbed upon silencing ATPase activity in γloop (Fig. 4), producing chlorophyll fluorescence patterns similar to *ptox2*. Unlike in γloop, the F_v/F_m in *ptox2* nearly returned to the reference strain level upon acetate consumption. This might be linked to PTOX1-dependent plastoquinone pool oxidation (SI Appendix, Fig. S11). If chlororespiration was indeed impaired in γloop, it might affect both PTOX1 and PTOX2. Unlike in dark-adapted *C. reinhardtii* wild type where PTOX2 cofractionates with membranes (50), the tethering of PTOX from vascular plants is facilitated upon illumination (51, 52). The authors showed that light-induced $\Delta\tilde{\mu}_{H^+}$ plays a role in PTOX binding to the plant thylakoid membrane. It remains to be tested whether the specific $\Delta\tilde{\mu}_{H^+\,dark}$ in γloop influences the amounts of soluble PTOX, which lack access to the plastoquinone pool. Thiol modulation of a C-terminal disulfide in PTOX that facilitates reversible dimerization in *A. thaliana* is missing in both PTOX isoforms from *C. reinhardtii* (53). Instead, when aligned with mitochondrial alternative oxidase (AOX), both algal PTOX isoforms harbor a cysteine in vicinity to the dubbed Cys-II, the latter playing a role in redox and metabolic AOX activity regulation (54). Whether factors like ATP, NADPH or other stromal metabolites in γloop have a regulatory effect on PTOX function remains to be tested.

Materials and Methods

Transformation and growth of *C. reinhardtii* strains

The transformation plasmid was published previously (19) and is based on the pPEARL expression vector (GenBank: KU531882.1). The *ATPC* CDS was cloned as a *Bam*HI/*Eco*RI fragment using ATPC.F forward (5'GTTCGAATTCATGGCCGCTATGCTCGCC) and reverse ATPC.R primers (5'GCCAGGATCCTTAGCCCGAGGTGGCGGCG). The hairpin that encodes the amino acids ^{254}GGEFA^{258} (*C. reinhardtii* numbering without acknowledging the *ATPC* transit peptide) was mutated using abutting primers hp.F (5'CAAGCTGACCGTGGAGCGCGAGAAGACC) and hp.R (5'CCCTCCTTGGTGGTCAGCTTGAAGATCTC), indicating underscored mismatches. The 323-bp PCR fragments of ATPC.R/hp2.F and the 775-bp fragment of ATPC.F/hp2.R were ligated, followed by another round of PCR using primers ATPC.F/ATPC.R. The redox-active cysteine couple was

disrupted by mutating one of the cysteines at position 203 to serine, using the CS.F (5'CCCATGGGCGAGCTGTCGGACGTGGACGGCAAG). The 406-bp PCR fragment of CS.F/ATPC.R was used in a megaprimer approach (55) to yield the mutated *ATPC* gene in combination with oligos ATPC.F/ATPC.R.

The recipient strain for nuclear transformation did not accumulate *ATPC* transcripts (56) and was cultured on acetate-supplemented TAP medium (57) due to lack of phototrophic growth. Transformants were obtained by electroporation (58) using 25 µF and 1000 V cm^{-1}. All successful transformants displayed phototrophic growth and were cultured under diurnal 16-h photoperiods of 50 µmol photons m^{-2} s^{-1} at 23°C on agar-supplemented and liquid Tris-minimal medium (TP) in the absence of acetate (57). Liquid cultures in the presence and absence of acetate were bubbled with sterile air and kept in the exponential phase (0.5–3 × 10^6 cells ml^{-1}) at 23°C by regular dilutions. Air bubbling ensured CO_2 supply for the Calvin-Benson-Bassham cycle. The experiments in Fig. 1 show the CC-5101 wild type strain. The CC-125 reference strain was used for experiments with *ptox2* mutants (50, 59).

Synchronized cultures (grown under 16-h photoperiods at 60 µmol photons m^{-2} s^{-1}) were used when incubating 400 × 10^6 cells in 400-mL culture volume of TP/TAP in a FMT 150 photobioreactor vessel supplied with sterile air (Photon Systems Instruments, Czech Republic). The culture was diluted to OD_{700} = 0.1 before two consecutive 16-h photoperiods (sigmoidal light 0-250 µmol photons m^{-2} s^{-1} white LEDs) that were followed by more than 48-h darkness at 23°C. TAP cultures were diluted again to OD_{700} = 0.1 after the first photoperiod. Chlorophyll fluorescence measurements were excited with blue LEDs to determine, via readouts of basal (F_0, F_s) and maximal fluorescence (F_m, F_m'), PSII quantum yields in the dark $(F_m-F_0)/F_m$, also referred to as F_v/F_m, as well as PSII quantum yields in the light $(F_m'-F_s)/F_m'$.

Cultivation of land plants

The *Arabidopsis thaliana* (Columbia ecotype) and *Pisum sativum* var. *arvense* were cultivated on soil at 23°C under diurnal 16-h photoperiods of 150 µmol photons m^{-2} s^{-1}. *Physcomitrium patens* Gransden wild type was grown at 23°C on $PpNO_3$ minimum medium (60) under diurnal 16-h photoperiods of 80 µmol photons m^{-2} s^{-1}. Leaves from *Ginkgo biloba*, *Sorghum bicolor*, and *Triticum aestivum* were obtained from the Botanical Garden of the University of Münster on August 1, 2018 (cloudy, 24°C).

In vivo spectroscopy

The electrochromic shift (ECS) of photosynthetic pigments was used to study the $\Delta\Psi$, the electric $\Delta\tilde{\mu}_{H^+}$ component (10, 11), by measuring the $\Delta I/I$ difference at wavelengths 520 nm – 546 nm in a Joliot-type spectrophotometer (JTS-10, Biologic, France, and JTS-150, Spectrologix, USA). The JTS-10 measurements in Fig. 1A used white pulsed LED detection light that was passed through respective interference filters (FWHM: 20 nm). In the other ECS measurements, the JTS-150 pulsed detection light originated from LEDs peaking at 520 and 546 nm, respectively. The light-detecting diodes were protected from scattered actinic light by 3-mm BG39 filters (Schott, Mainz, Germany). Illumination of the samples was interrupted by short dark intervals (250 µs) during which 10-µs detecting pulses were placed after 200 µs. All shown kinetics were obtained in the presence of photosystem (PS) II activity but for comparison reasons the ECS signals were normalized to PSI, i.e., the $\Delta I/I$ (520 nm – 546 nm) produced by 1 PSI charge separation in a separate calibration measurement (reviewed in 12). To do so, a saturating 6-ns laser flash was delivered at 700 nm (Q-switched Nd:YAG, Continuum, USA) in the presence of 1 mM hydroxylamine and 10 µM 3-(3,4-dichlorophenyl)-1,1-dimethylurea to inhibit PSII in the algal samples (see SI Appendix, Fig. S12 for algal PSI-related $\Delta I/I$ comparison per chlorophyll). In Fig. 1A, it was assumed that land plant PSI and PSII equally contributed to the fast ECS generation upon a laser flash, therefore the flash-induced $\Delta I/I$ before the first detection at ~500-µs was equal to 2 PSI charge separations.

Short saturating light pulses with a duration of several ms were used to drive multiple turnovers of the entire photosynthetic chain until a plateau-like $\Delta\Psi$ was reached (27, 36). Extending the pulse beyond that point would result in ECS inversion due to ΔpH formation which was avoided by switching off the light. The following $\Delta\Psi$ consumption was CF_1F_o-related and detected as ECS signals returning to the baseline. The latter corresponds to the dark-equilibrated $\Delta\tilde{\mu}_{H^+}$ ($\Delta\tilde{\mu}_{H^+\text{dark}}$), which was not affected by the light perturbations when spacing repetitive measurements by at least 2 min darkness. The ECS signal during a pulse vary in amplitude depending on (*i*) technical and (*ii*) physiological parameters (27, 36). (*i*) The ECS peak amplitude increases with pulse light intensity, which was provided by 630-nm LEDs set to 600 mA in the main text. The same relationship holds for the ECS decay amplitude during the first ~10 ms after the pulse. However, the subsequent signal amplitude decaying from 10 ms darkness to the baseline $\Delta\tilde{\mu}_{H^+\text{dark}}$ were independent from the light intensity (SI Appendix, Fig. S4C; for the dependency of this amplitude though, see (*ii*) below). Thus, the measured ECS at 10 ms after the pulse (ECS_{10ms}) marks a technical reference for light-induced $\Delta\Psi$ changes with respect to $\Delta\tilde{\mu}_{H^+\text{dark}}$. (*ii*) The absolute value of the $\Delta\tilde{\mu}_{H^+\text{dark}}$ is obscure and a result of cellular physiology. This can be demonstrated by collapsing $\Delta\tilde{\mu}_{H^+\text{dark}}$ upon treatments with respiration inhibitors or uncouplers (SI Appendix, Figs. S4A-B, S4D) which produced larger pulse-induced signals between $\Delta\tilde{\mu}_{H^+\text{dark}}$ (baseline) and ECS_{10ms} (technical reference). To circumvent this physiological obstruction, the unknown $\Delta\tilde{\mu}_{H^+\text{dark}}$ was expressed as negative units relative to the technical reference by setting ECS_{10ms} to 0 PSI charge separations. We resort to this representation in the main text since the alternative approach (measure non-inhibited samples upon dark incubation first, then determine absolute $\Delta\tilde{\mu}_{H^+\text{dark}}$ upon inhibitor/uncoupler treatment) is time-consuming and prone to variable metabolic coupling between energy transducing organelles (27, 61).

The decay kinetics between ECS_{10ms} and $\Delta\tilde{\mu}_{H^+\text{dark}}$ was quantified using the two-exponential function $y = y_0 + A_1 e^{-(x-x_0)/t_1} + A_2 e^{-(x-x_0)/t_2}$. Using OriginPro software, x_0 was fixed to 10 ms, the calculated y_0 closely resembled $\Delta\tilde{\mu}_{H^+\text{dark}}$, and A_1 (t_1) and A_2 (t_2) correspond to the amplitudes (decay constant) of fast and slow decay phase, respectively (for replicate kinetics and fitted curves see SI Appendix, Fig. S5). The function describes two different CF_1F_o activity states (37, 38): The first one was activated by $\Delta\tilde{\mu}_{H^+}$ provided by the pulse, whereas the second one was not. Fig. 2D shows $-A_1$ which marked the $\Delta\tilde{\mu}_{H^+}$ threshold with respect to ECS_{10ms} under which CF_1F_o transitioned to a less active form.

Acknowledgments

We thank Prof. Michael Hippler for helpful discussions. F.B. acknowledges Deutsche Forschungsgemeinschaft (DFG, German Research Foundation) – 461765884, 507704013.

References

1. F. Buchert, "Chapter Three - Chloroplast ATP synthase from green microalgae" in Advances in Botanical Research, T. Hisabori, Ed. (Academic Press, 2020), vol. 96, pp. 75-118.
2. W. Junge, N. Nelson, ATP synthase. *Annu. Rev. Biochem.* **84**, 631-657 (2015).
3. J. H. Kaplan, E. Uribe, A. T. Jagendorf, ATP hydrolysis caused by acid-base transition of spinach chloroplasts. *Arch Biochem Biophys* **120**, 365-370 (1967).
4. P. Gräber, H. T. Witt, Relations between the electrical potential, pH gradient, proton flux and phosphorylation in the photosynthetic membrane. *Biochim. Biophys. Acta* **423**, 141-163 (1976).

5. D. A. Harris, A. R. Crofts, The initial stages of photophosphorylation. Studies using excitation by saturating, short flashes of light. *Biochim. Biophys. Acta* **502**, 87-102 (1978).
6. D. M. Kramer, A. R. Crofts, Activation of the chloroplast ATPase measured by the electrochromic change in leaves of intact plants. *Biochimica et Biophysica Acta* **976**, 28-41 (1989).
7. A. Hahn, J. Vonck, D. J. Mills, T. Meier, W. Kuhlbrandt, Structure, mechanism, and regulation of the chloroplast ATP synthase. *Science* **360** (2018).
8. J. H. Yang, D. Williams, E. Kandiah, P. Fromme, P. L. Chiu, Structural basis of redox modulation on chloroplast ATP synthase. *Communications biology* **3**, 482 (2020).
9. P. D. Boyer, The binding change mechanism for ATP synthase - some probabilities and possibilities. *Biochim. Biophys. Acta* **1140**, 215-250 (1993).
10. W. Junge, H. T. Witt, On the ion transport system of photosynthesis--investigations on a molecular level. *Z Naturforsch B* **23**, 244-254 (1968).
11. H. T. Witt, Energy conversion in the functional membrane of photosynthesis. Analysis by light pulse and electric pulse methods. The central role of the electric field. *Biochim. Biophys. Acta* **505**, 355-427 (1979).
12. B. Bailleul, P. Cardol, C. Breyton, G. Finazzi, Electrochromism: a useful probe to study algal photosynthesis. *Photosynthesis Res.* **106**, 179-189 (2010).
13. A. Krieger, E. Weis, The role of calcium in the pH-dependent control of Photosystem II. *Photosynth Res* **37**, 117-130 (1993).
14. I. Zaharieva, J. M. Wichmann, H. Dau, Thermodynamic limitations of photosynthetic water oxidation at high proton concentrations. *J. Biol. Chem.* **286**, 18222-18228 (2011).
15. K. K. Niyogi, T. B. Truong, Evolution of flexible non-photochemical quenching mechanisms that regulate light harvesting in oxygenic photosynthesis. *Curr. Opin. Plant Biol.* **16**, 307-314 (2013).
16. G. A. Davis *et al.*, Limitations to photosynthesis by proton motive force-induced photosystem II photodamage. *Elife* **5** (2016).
17. U. Armbruster *et al.*, Ion antiport accelerates photosynthetic acclimation in fluctuating light environments. *Nat Commun* **5**, 5439 (2014).
18. A. Herdean *et al.*, A voltage-dependent chloride channel fine-tunes photosynthesis in plants. *Nat Commun* **7**, 11654 (2016).
19. F. Buchert, B. Bailleul, T. Hisabori, A γ-subunit point mutation in *Chlamydomonas reinhardtii* chloroplast F_1F_o-ATP synthase confers tolerance to reactive oxygen species. *Biochim. Biophys. Acta* **1858**, 966-974 (2017).
20. K. Kohzuma *et al.*, The long-term responses of the photosynthetic proton circuit to drought. *Plant Cell Environ.* **32**, 209-219 (2009).
21. A. Kanazawa, D. M. Kramer, *In vivo* modulation of nonphotochemical exciton quenching (NPQ) by regulation of the chloroplast ATP synthase. *Proc. Natl. Acad. Sci. USA* **99**, 12789-12794 (2002).
22. B. Naranjo *et al.*, The chloroplast NADPH thioredoxin reductase C, NTRC, controls non-photochemical quenching of light energy and photosynthetic electron transport in Arabidopsis. *Plant Cell Environ* **39**, 804-822 (2016).
23. J. D. Mills, P. Mitchell, P. Schurmann, Modulation of coupling factor ATPase activity in intact chloroplasts - The role of the thioredoxin system. *FEBS Lett.* **112**, 173-177 (1980).
24. L. R. Carrillo, J. E. Froehlich, J. A. Cruz, L. J. Savage, D. M. Kramer, Multi-level regulation of the chloroplast ATP synthase: the chloroplast NADPH thioredoxin reductase C (NTRC) is required for redox modulation specifically under low irradiance. *Plant J.* **87**, 654-663 (2016).
25. K. Yoshida, A. Hara, K. Sugiura, Y. Fukaya, T. Hisabori, Thioredoxin-like2/2-Cys peroxiredoxin redox cascade supports oxidative thiol modulation in chloroplasts. *Proc. Natl. Acad. Sci. USA* **115**, E8296-E8304 (2018).
26. U. Junesch, P. Gräber, Influence of the redox state and the activation of the chloroplast ATP synthase on proton-transport-coupled ATP synthesis hydrolysis. *Biochim. Biophys. Acta* **893**, 275-288 (1987).

27. F. Buchert, B. Bailleul, P. Joliot, Disentangling chloroplast ATP synthase regulation by proton motive force and thiol modulation in Arabidopsis leaves. *Biochim. Biophys. Acta* **1862**, 148434 (2021).
28. K. Akiyama *et al.*, Two specific domains of the gamma subunit of chloroplast F(o)F(1) provide redox regulation of the ATP synthesis through conformational changes. *Proc Natl Acad Sci U S A* **120**, e2218187120 (2023).
29. G. Wu, D. R. Ort, Mutation in the cysteine bridge domain of the γ subunit affects light regulation of the ATP synthase but not photosynthesis or growth in Arabidopsis. *Photosynthesis Res.* **97**, 185-193 (2008).
30. S. A. Ross, M. X. Zhang, B. R. Selman, Role of the *Chlamydomonas reinhardtii* coupling factor-1 γ subunit cysteine bridge in the regulation of ATP synthase. *J. Biol. Chem.* **270**, 9813-9818 (1995).
31. D. R. Ort, K. Oxborough, *In situ* regulation of chloroplast coupling factor activity. *Annu. Rev. Plant Physiol. Plant Mol. Biol.* **43**, 269-291 (1992).
32. S. M. Theg, K. Cline, G. Finazzi, F. A. Wollman, The energetics of the chloroplast Tat protein transport pathway revisited. *Trends Plant Sci.* **10**, 153-154 (2005).
33. W. J. Nawrocki, N. J. Tourasse, A. Taly, F. Rappaport, F. A. Wollman, The plastid terminal oxidase: its elusive function points to multiple contributions to plastid physiology. *Annu. Rev. Plant Biol.* **66**, 49-74 (2015).
34. F. Rappaport, G. Finazzi, Y. Pierre, P. Bennoun, A new electrochemical gradient generator in thylakoid membranes of green algae. *Biochemistry* **38**, 2040-2047 (1999).
35. K. Kohzuma *et al.*, Thioredoxin-insensitive plastid ATP synthase that performs moonlighting functions. *Proc. Natl. Acad. Sci. USA* **109**, 3293-3298 (2012).
36. P. Joliot, A. Joliot, Quantification of the electrochemical proton gradient and activation of ATP synthase in leaves. *Biochim. Biophys. Acta* **1777**, 676-683 (2008).
37. W. Junge, The critical electric potential difference for photophosphorylation. Its relation to the chemiosmotic hypothesis and to the triggering requirements of the ATPase system. *Eur. J. Biochem.* **14**, 582-592 (1970).
38. W. Junge, B. Rumberg, H. Schroder, The necessity of an electric potential difference and its use for photophosphorylation in short flash groups. *Eur. J. Biochem.* **14**, 575-581 (1970).
39. M. Á. Ruiz-Sola *et al.*, Light-independent regulation of algal photoprotection by CO2 availability. *Nature Communications* **14**, 1977 (2023).
40. E. Wientjes, H. van Amerongen, R. Croce, Quantum Yield of Charge Separation in Photosystem II: Functional Effect of Changes in the Antenna Size upon Light Acclimation. *The Journal of Physical Chemistry B* **117**, 11200-11208 (2013).
41. M. F. Hohmann-Marriott, K. Takizawa, J. J. Eaton-Rye, L. Mets, J. Minagawa, The redox state of the plastoquinone pool directly modulates minimum chlorophyll fluorescence yield in Chlamydomonas reinhardtii. *FEBS Lett.* **584**, 1021-1026 (2010).
42. F. Buchert, F. Zito, "Chapter 17 - Chloroplast ATP synthase and the cytochrome b_6f complex" in The Chlamydomonas Sourcebook (Third Edition), A. R. Grossman, F.-A. Wollman, Eds. (Academic Press, London, 2023), https://doi.org/10.1016/B978-0-12-821430-5.00020-1, pp. 561-589.
43. T. Sekiguchi *et al.*, Chloroplast ATP synthase is reduced by both *f*-type and *m*-type thioredoxins. *Biochim. Biophys. Acta* **1861**, 148261 (2020).
44. J. M. Zhou, Z. X. Xue, Z. Y. Du, T. Melese, P. D. Boyer, Relationship of tightly bound ADP and ATP to control and catalysis by chloroplast ATP synthase. *Biochemistry* **27**, 5129-5135 (1988).
45. Y. Kim, H. Konno, Y. Sugano, T. Hisabori, Redox regulation of rotation of the cyanobacterial F_1-ATPase containing thiol regulation switch. *J. Biol. Chem.* **286**, 9071-9078 (2011).
46. H. Strotmann, N. Shavit, S. Leu, "Assembly and Function of the Chloroplast ATP Synthase" in The Molecular Biology of Chloroplasts and Mitochondria in

527 Chlamydomonas, J. D. Rochaix, M. Goldschmidt-Clermont, S. Merchant, Eds. (Springer
528 Netherlands, Dordrecht, 1998), 10.1007/0-306-48204-5_25, pp. 477-500.
529 47. F. Jans *et al.*, A type II NAD(P)H dehydrogenase mediates light-independent
530 plastoquinone reduction in the chloroplast of *Chlamydomonas*. *Proc Natl Acad Sci U S A*
531 **105**, 20546-20551 (2008).
532 48. X. Johnson, J. Alric, Central carbon metabolism and electron transport in
533 *Chlamydomonas reinhardtii*: metabolic constraints for carbon partitioning between oil and
534 starch. *Eukaryot. Cell* **12**, 776-793 (2013).
535 49. L. Cournac *et al.*, In vivo interactions between photosynthesis, mitorespiration, and
536 chlororespiration in Chlamydomonas reinhardtii. *Plant Physiol.* **129**, 1921-1928 (2002).
537 50. W. J. Nawrocki *et al.*, Chlororespiration controls growth under intermittent light. *Plant*
538 *Physiol.* **179**, 630-639 (2019).
539 51. K. Feilke *et al.*, Effect of Chlamydomonas plastid terminal oxidase 1 expressed in
540 tobacco on photosynthetic electron transfer. *Plant J.* **85**, 219-228 (2016).
541 52. S. Bolte *et al.*, Dynamics of the localization of the plastid terminal oxidase inside the
542 chloroplast. *J. Exp. Bot.* **71**, 2661-2669 (2020).
543 53. I. Rog, A. K. Chaturvedi, V. Tiwari, A. Danon, Low light-regulated intramolecular disulfide
544 fine-tunes the role of PTOX in Arabidopsis. *Plant J.* **109**, 585-597 (2022).
545 54. J. Selinski *et al.*, Alternative Oxidase Isoforms Are Differentially Activated by Tricarboxylic
546 Acid Cycle Intermediates. *Plant Physiol.* **176**, 1423-1432 (2018).
547 55. O. Landt, H. P. Grunert, U. Hahn, A general method for rapid site-directed mutagenesis
548 using the polymerase chain reaction. *Gene* **96**, 125-128 (1990).
549 56. D. Drapier, B. Rimbault, O. Vallon, F. A. Wollman, Y. Choquet, Intertwined translational
550 regulations set uneven stoichiometry of chloroplast ATP synthase subunits. *EMBO J.* **26**,
551 3581-3591 (2007).
552 57. D. S. Gorman, R. P. Levine, Cytochrome *f* and plastocyanin: their sequence in the
553 photosynthetic electron transport chain of *Chlamydomonas reinhardtii*. *Proc Natl Acad*
554 *Sci U S A* **54**, 1665-1669 (1965).
555 58. C. Raynaud *et al.*, Evidence for regulatory function of nucleus-encoded factors on mRNA
556 stabilization and translation in the chloroplast. *Proc Natl Acad Sci U S A* **104**, 9093-9098
557 (2007).
558 59. L. Houille-Vernes, F. Rappaport, F. A. Wollman, J. Alric, X. Johnson, Plastid terminal
559 oxidase 2 (PTOX2) is the major oxidase involved in chlororespiration in Chlamydomonas.
560 *Proc Natl Acad Sci U S A* **108**, 20820-20825 (2011).
561 60. N. W. Ashton, N. H. Grimsley, D. J. Cove, Analysis of gametophytic development in the
562 moss, Physcomitrella patens, using auxin and cytokinin resistant mutants. *Planta* **144**,
563 427-435 (1979).
564 61. B. Bailleul *et al.*, Energetic coupling between plastids and mitochondria drives CO_2
565 assimilation in diatoms. *Nature* **524**, 366-369 (2015).

566

Figures

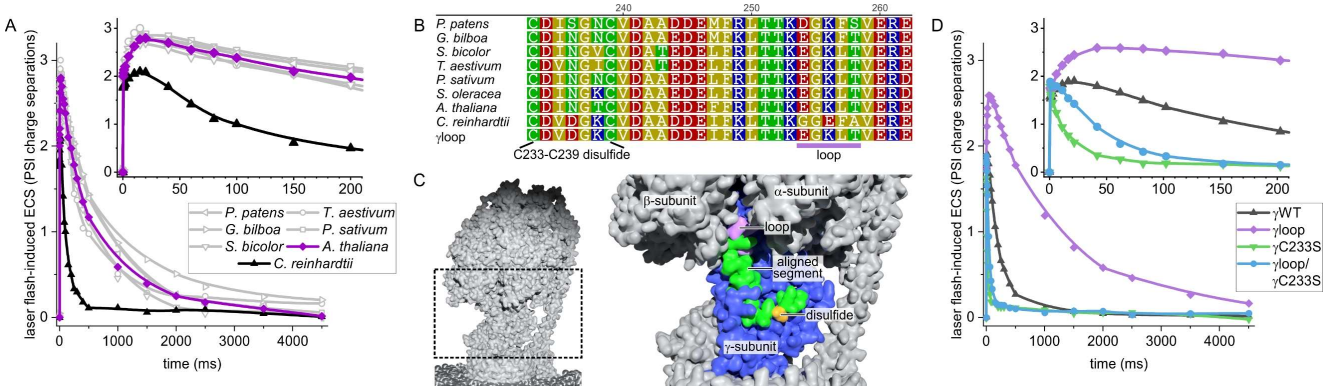

Figure 1. A loop segment in the algal γ-subunit redox domain determines laser flash-induced decay kinetics of the ECS signal upon dark adaptation. (*A*) Decay of ECS kinetics was measured in dark-adapted *C. reinhardtii* and various land plant species. (*B*) The partial γ-subunit redox domain sequence alignment of species from panel *A* highlight the varied loop segment that was exchanged in γloop algal mutants (*C. reinhardtii* numbering on top). (*C*) The rotating loop segment is inserted in between the $\alpha_3\beta_3$ hexamer, shown here for spinach CF_1F_o (PDB ID: 6FKH). (*D*) CF_1F_o was analyzed in photoautotrophic algal cultures via flash-induced ECS decay measurements. Besides plant-like γloop mutants the analysis also involved two γC233S disulfide mutants in the presence of both loop variations (see SI Appendix, Fig. S1 for biological replicates).

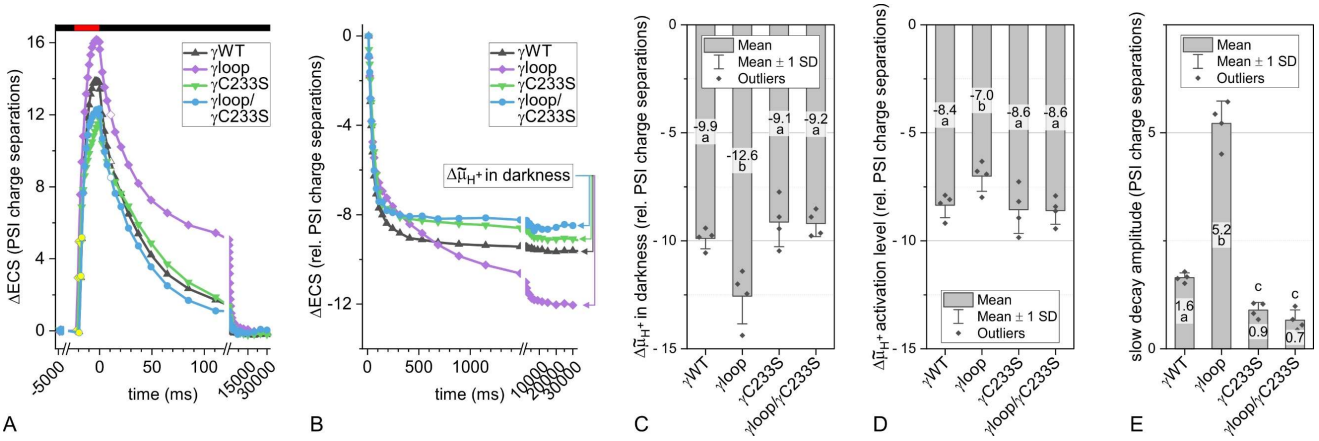

Figure 2. Optical measurements of the $\Delta\tilde{\mu}_{H^+}$ in the dark reveal lower values in the CF_1F_o γloop mutant due to its elevated activation threshold. (*A*) The increase of the ECS by a light pulse (red bar) as well as the ECS decay in dark (black bar) is shown in samples from Fig. 1D. Linear initial ECS generation was quantified from yellow symbols (see SI Appendix, Fig. S3). To deconvolute the variable ECS baseline level, the technical ECS reference at 10 ms after the pulse (white symbols) was used. (*B*) This reference was set to 0 for expressing the individual $\Delta\tilde{\mu}_{H^+}$ in darkness and comparing the multiphasic ECS decay. (*C*) The averaged $\Delta\tilde{\mu}_{H^+}$ in darkness is shown (N = 4 ± SD, One-Way ANOVA/Fisher-LSD, P<0.05). (*D*) ECS decay kinetics from panel *B* were fit with a two-exponential (see SI Appendix, Fig. S5 for biological replicates) and the averaged $\Delta\tilde{\mu}_{H^+}$ activation level is shown that separated the fast from the slow decay phase. (*E*) The averaged amplitudes of the slow ECS decay phase are shown.

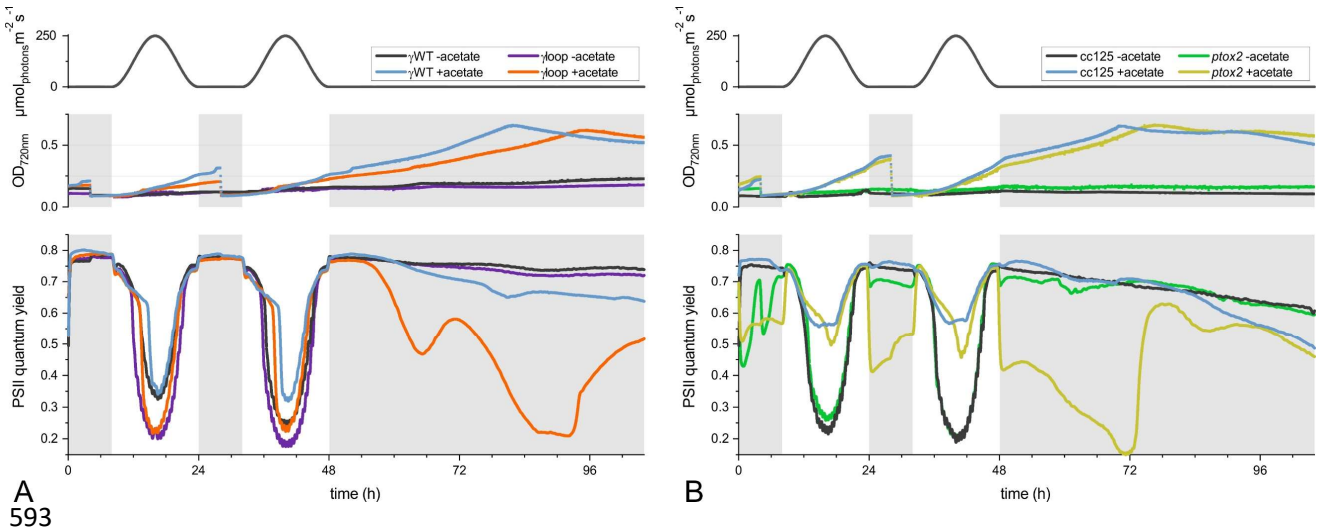

Figure 3. Algal photobioreactor experiments show two light cycles and exposure to extended darkness. (*A*) The OD_{720nm} turbidity, adjusted during the first night cycle (and second in the presence of acetate), as well as the PSII quantum yields are shown for CF_1F_o variants γWT and γloop mutant at a given light intensity. (*B*) The same experiment is shown for CC-125 and *ptox2* (see SI Appendix, Figs. S7 and S10 for replicates).

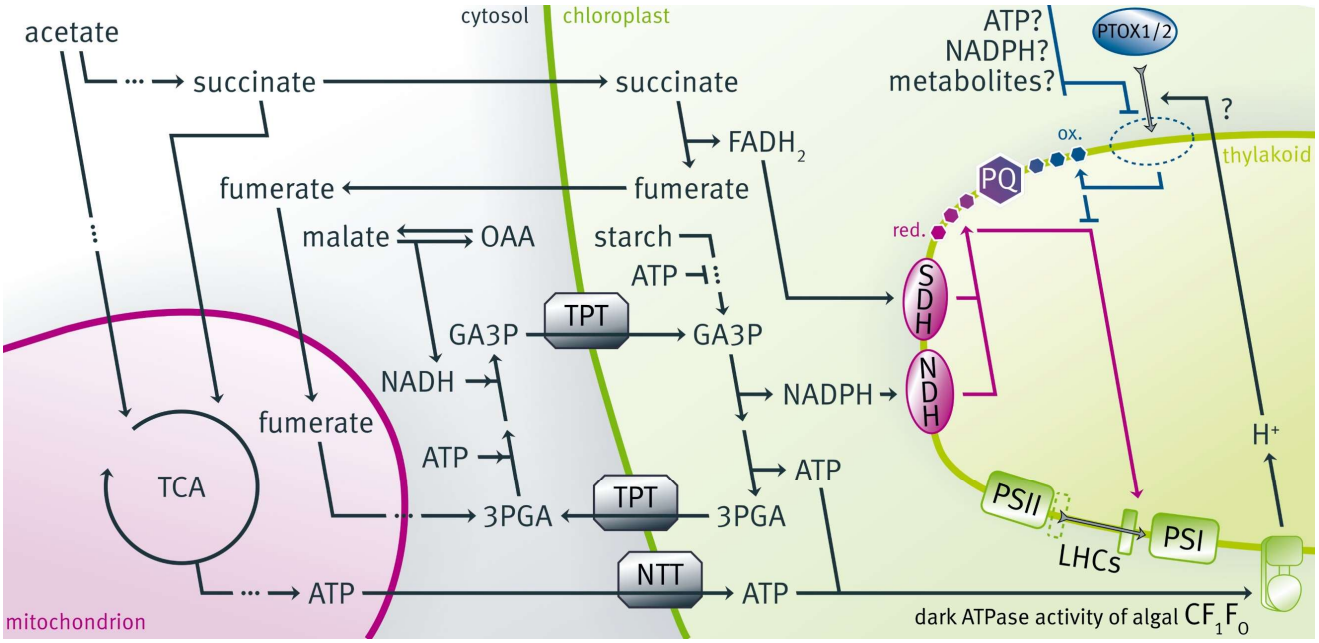

Figure 4. A tentative model is shown of acetate-dependent plastoquinone pool reduction in the absence of dark ATPase activity. Stromal and/or trans-thylakoid determinants might affect PTOX1 and PTOX2 activities in the γloop variant of CF_1F_o. The selected metabolic fluxes in *C. reinhardtii* are reviewed in Ref. 48. 3PGA: 3-phosphoglycerate; GA3P: glyceraldehyde 3-phosphate; LHC, light harvesting complex; NDH, NADPH dehydrogenase; NTT, nucleotide triphosphate transporter; OAA, oxaloacetate; PQ, plastoquinone/plastoquinol; PSI/PSII, photosystem I/II; PTOX, plastid terminal oxidase; SDH, succinate dehydrogenase; TPT, triose phosphate/phosphate translocator.

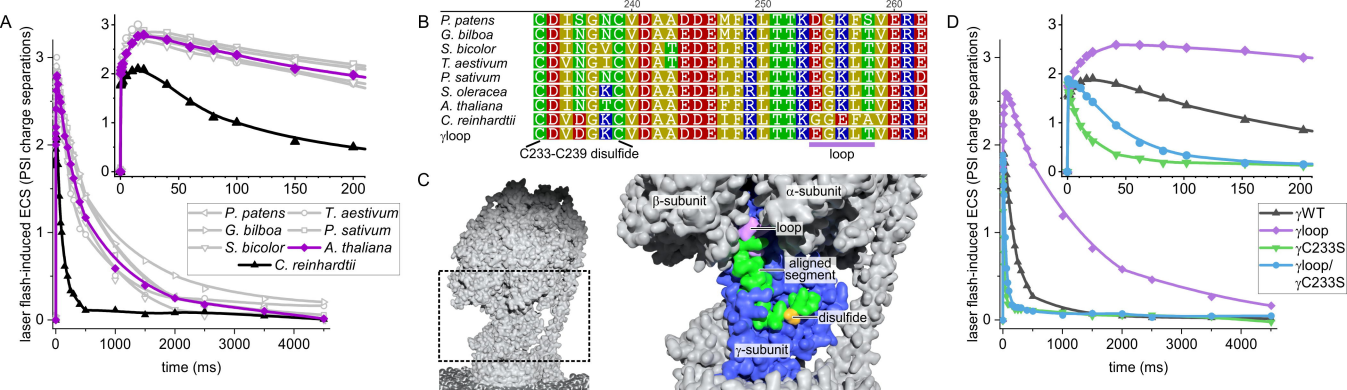
A
laser flash-induced ECS (PSI charge separations)
time (ms)
P. patens
G. bilboa
S. bicolor
T. aestivum
P. sativum
A. thaliana
C. reinhardtii
B
240
250
260
P. patens
G. bilboa
S. bicolor
T. aestivum
P. sativum
S. oleracea
A. thaliana
C. reinhardtii
γloop
C233-C239 disulfide
loop
C
β-subunit
α-subunit
loop
aligned segment
disulfide
γ-subunit
D
laser flash-induced ECS (PSI charge separations)
time (ms)
γWT
γloop
γC233S
γloop/ γC233S

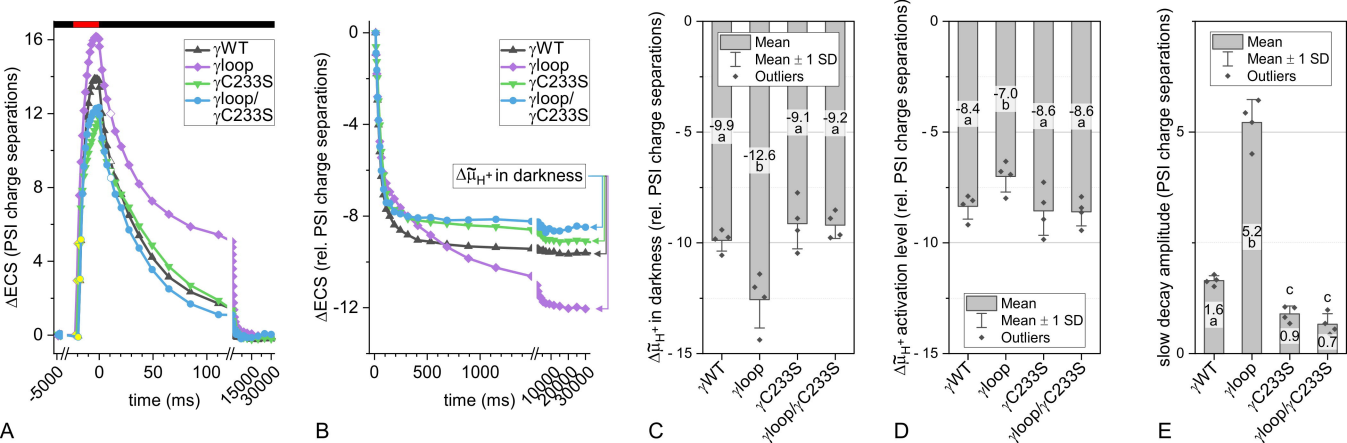
A
ΔECS (PSI charge separations)
time (ms)
γWT
γloop
γC233S
γloop/
γC233S
B
ΔECS (rel. PSI charge separations)
time (ms)
Δμ̃H+ in darkness
C
Δμ̃H+ in darkness (rel. PSI charge separations)
Mean
Mean ± 1 SD
Outliers
-9.9
a
-12.6
b
-9.1
a
-9.2
a
D
Δμ̃H+ activation level (rel. PSI charge separations)
-8.4
a
-7.0
b
-8.6
a
-8.6
a
E
slow decay amplitude (PSI charge separations)
1.6
a
5.2
b
0.9
c
0.7
c

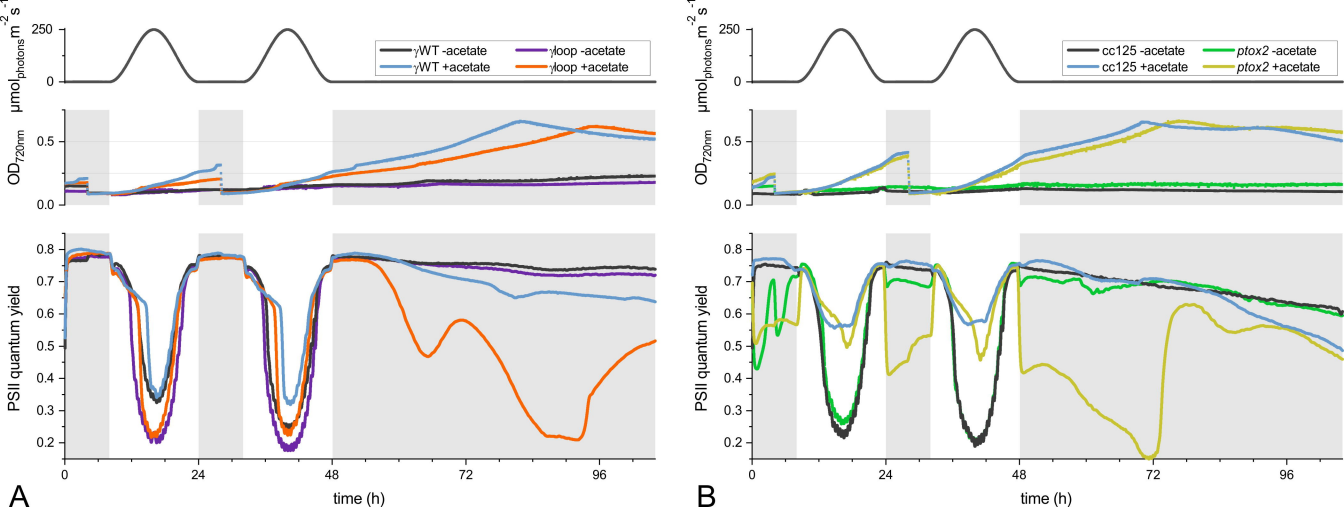
µmol photons m-2 s-1
250
0
γWT -acetate
γWT +acetate
γloop -acetate
γloop +acetate
OD720nm
0.5
0.0
PSII quantum yield
0.8
0.7
0.6
0.5
0.4
0.3
0.2
0
24
48
72
96
time (h)
A
cc125 -acetate
cc125 +acetate
ptox2 -acetate
ptox2 +acetate
B

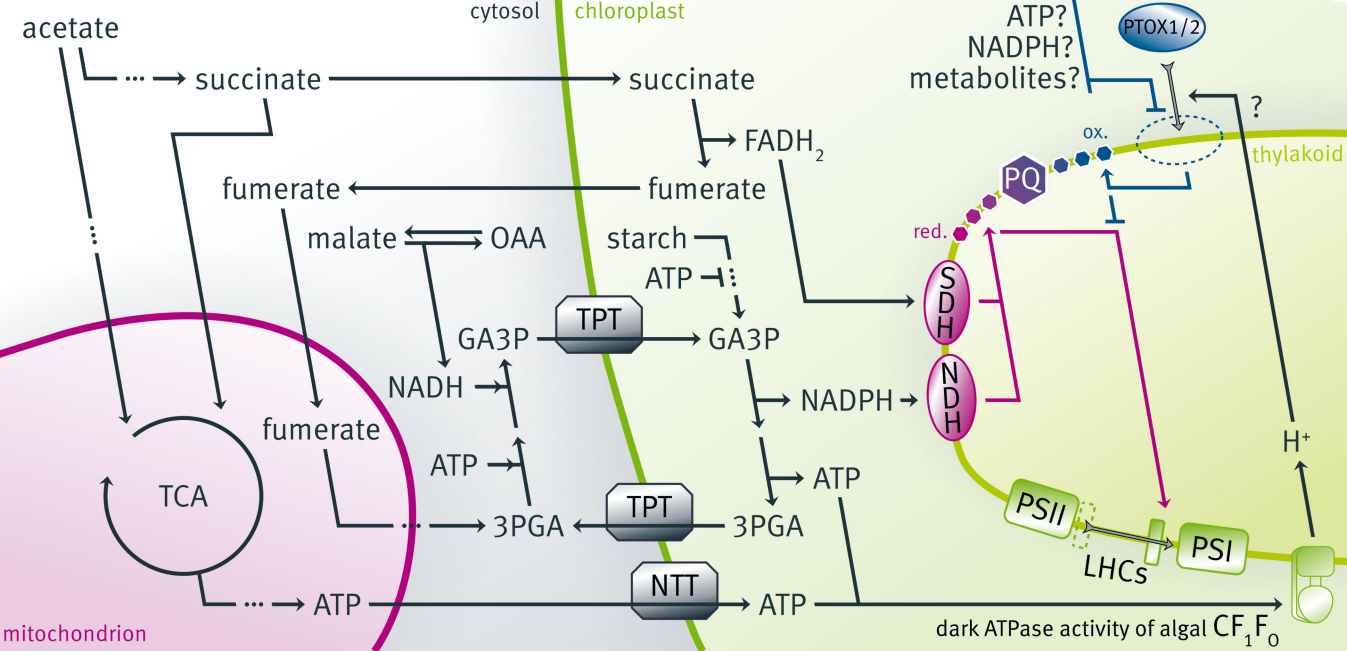
cytosol
chloroplast
acetate
succinate
succinate
FADH2
fumerate
fumerate
malate
OAA
starch
ATP
GA3P
TPT
GA3P
NADH
NADPH
fumerate
ATP
ATP
TCA
3PGA
TPT
3PGA
ATP
NTT
ATP
mitochondrion
ATP?
NADPH?
metabolites?
PTOX1/2
?
ox.
thylakoid
PQ
red.
SDH
NDH
H+
PSII
PSI
LHCs
dark ATPase activity of algal CF1F0